

A PARALLEL SOLVER WITH MULTIPHYSICS FINITE ELEMENT METHOD FOR POROELASTICITY COUPLED WITH ELASTICITY MODEL*

ZHIHAO GE[†] AND CHENGXIN WANG[‡]

Abstract. In this paper, we propose a parallel solver for solving the quasi-static linear poroelasticity coupled with linear elasticity model in the Lagrange multiplier framework. Firstly, we reformulate the model into a coupling of the nearly incompressible elasticity and an unsteady affection-diffusion equations by setting new variable “elastic pressure” and “volumetric fluid content”. And we introduce a Lagrange multiplier to guarantee the normal stress continuity on the interface. Then, we give the variational formulations in each subdomain and choose the \mathbf{P}_k - P_1 - P_1 mixed finite element tuple for poroelasticity subdomain, and \mathbf{P}_k - P_1 finite element pair ($k = 1, 2$) for elasticity subdomain and the backward Euler scheme for time. Also, we propose a parallel solver for solving the fully discrete scheme at each time step— the FETI method with a classical FETI preconditioner for solving the Lagrange multiplier and calculating the subproblems in each subdomain in parallel. And we show several numerical tests to validate the computational efficiency and the convergence error order, and we consider Barry-Mercer’s model as the benchmark test to show that there no oscillation in the computed pressure. Finally, we draw conclusions to summarize the main results of this paper.

Key words. Poroelasticity, elasticity, multiphysics finite element method, domain decomposition, Schur complement method, FETI method

AMS subject classifications. 65N30.

1. Introduction. In this paper, we study the non-overlapping coupled poroelasticity and elasticity model, which is a challenging multiphysics and multidomain problem with applications to multiple industrial sectors. One typical practical usage is the simulation to the reservoir[1, 8, 10]. For example, attaching increasing importance to energy conservation and carbon reduction, the carbon dioxide underground injection sequestration techniques, as an efficient selection for reducing the greenhouse gases in the atmosphere, is now a popular research topic, in which one of the motivation is that the supercritical CO₂ fracturing has better performance in fluid fracturing and oil production than hydraulic fracturing. In addition, the model of coupled poroelasticity and elasticity can be applied in the biomechanical engineering[5, 25], such as simulation of the brain injury and tumor growth.

The coupled poroelasticity and elasticity model consists of at least two different subdomains, that is, the poroelastic “pay-zone” and elastic “nonpay-zone”. We adopt the Biot’s[3, 24] system of poroelasticity to model the poroelastic media in the pay-zone and a classic elasticity model in the nonpay-zone. The coupled model can be seen as an elastic model in which part of the domain has a porous structure and is saturated by a fluid[7]. For the respective models in each subdomain.

The coupled poroelasticity and elasticity model was first studied by Girault et al[11], in which the displacement \mathbf{u} was partitioned into two parts, one of which is dependent on the fluid pressure p and the other is independent. And for the numerical study, the discontinuous Galerkin jumps and mortars method was adopted for semi-discretizing the model, and the corresponding error estimates was given. A Mandel’s model was studied as a numerical example, in which the errors of the model with its order were validated.

In practical actuality, various discretization schemes of the coupled poroelasticity and elasticity model can be chosen. For the model of poroelasticity, Phillips and Wheeler[21, 22] proposed a mixed finite element method for solving a quasi-linear model of poroelasticity. However, the tendency of Lamé constant to infinity $\lambda \rightarrow \infty$ will lead to a so-called locking phenomenon, that is, the solution will lose convergence if λ is set to be sufficiently large. To overcome the locking, one of the efficient way is to adopt the discontinuous Galerkin method[23]. Another strategy is the multiphysics finite element method[9], where two new variables were introduced so that the elastic momentum balance part was rewritten in a generalized Stokes form, and validated the absence of locking by some numerical examples.

The main motivation for studying various coupled model is to adopt alternating parallelized algorithms to improve the calculation efficiency. Combining with suitable domain decomposition frameworks, we can partition

*LAST UPDATE: September 9, 2025

[†]School of Mathematics and Statistics, Henan University, Kaifeng 475004, PR China (Email: zhihaoge@henu.edu.cn). The work of this author was supported by National Natural Science Foundation of China(No. 12371393) and Natural Science Foundation of Henan Province(No. 242300421047).

[‡]School of Mathematics and Statistics, Henan University, Kaifeng 475004, P.R. China.

the domain into several solvable subdomains with suitable transmission conditions[19]. For example, the study in [11] introduced the model on the Steklov-Poincaré framework, which suggests various iterative algorithms for its solution, such as Dirichlet-Neumann method, Neumann-Neumann method and etc.. In this paper we adopt the Lagrange multiplier framework, that is, we introduced the normal stress on the interface from both subdomains as a unknown Lagrange multiplier variable $\boldsymbol{\lambda}$, and construct a saddle point system, where we can utilize the algorithms for iterating the Lagrange multiplier to approximate the transmission conditions, such as Uzawa's algorithm[13,20], non-overlapping Schwarz method[2,17,18], finite element tearing and interconnecting(FETI) method[6,14–16] and etc..

In this paper, we adopt FETI method to solve the coupled poroelasticity and elasticity model with multiphysics finite element approximation, which will be presented in the rest of this paper organized in several sections. In ?? we present the coupled poroelasticity and elasticity model in a Lagrange multiplier framework, where the normal stress on the interface is introduced as the Lagrange multiplier term, then we reformulate the model by introducing new variables. Variational formulation and the corresponding semi-discretization of the reformulated model is given, in which a \mathbf{P}_2 - P_1 - P_1 - P_1 finite element method and a \mathbf{P}_2 - P_1 finite element method is chosen for the discretization, and we proved the existence and uniqueness of solutions to the model in each subdomain, and prescribed the equivalence of solution between coupled model and decoupled sub-models. In ?? , a fully-discrete scheme is proposed by adopting the backward-Euler time-advancing method, which can be seen as a saddle point problem at each time step. Finally, in ?? , several benchmark numerical experiments are provided to show the performance of the proposed approach and methods.

2. The Coupled Poroelasticity and Elasticity Model. Consider a bounded polygonal domain $\Omega \subset \mathbb{R}^d$ ($d = 2, 3$) with the continuous boundary $\partial\Omega$. Suppose that Ω is partitioned into two non-overlapping subdomains Ω^P, Ω^E , which represents the quasi-static poroelastic reservoir layer and the elastic caprock layer respectively:

$$\overline{\Omega} = \overline{\Omega^P \cup \Omega^E}, \quad \Omega^P \cap \Omega^E = \emptyset.$$

In this paper we use the appellation to each region in [11], that is, the porous “pay-zone” and non-porous “nonpay-zone”. The pay-zone Ω^P satisfies consolidation model for a linear elastic, homogeneous, isotropic, porous solid media saturated with a slightly compressible fluid. The nonpay-zone Ω^E , a linear elasticity model will be adopted. For convenience when describing the finite element approximation, we assume that the domain Ω is a bounded polygon with boundary $\partial\Omega$ and interface $\Gamma = \overline{\Omega^P} \cap \overline{\Omega^E}$. For any variable \mathcal{G} , let $\mathcal{G}_{\mathcal{D}} := \mathcal{G}|_{\Omega^{\mathcal{D}}}$ ($\mathcal{D} = P, E$) denotes its restriction in subdomain $\Omega^{\mathcal{D}}$ (unless an extra description is given, we will use the superscript notation \mathcal{D} to represent either subdomain through this paper). The normal vectors \mathbf{n}_P , \mathbf{n}_E , $\mathbf{n}_{P \rightarrow E}$ and $\mathbf{n}_{E \rightarrow P}$ are as shown in Figure 2.1.

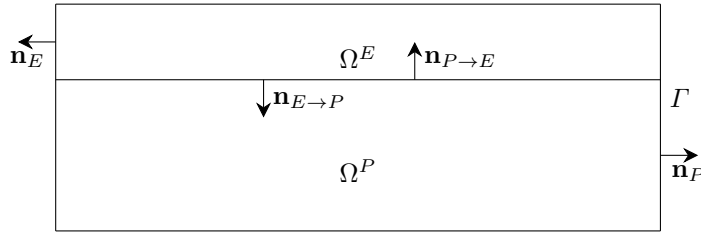


Figure 2.1: A top-bottom coupled structure of domains.

2.1. Governing Equations. In this paper, we consider the quasi-static poroelasticity model in Ω^P and elasticity in Ω^E interconnected by the interface Γ [11, 21, 22]: Find $\mathbf{u}_p, \mathbf{u}_E, p$ for all $T > 0$ such that

$$-\operatorname{div} \boldsymbol{\sigma}_P(\mathbf{u}_P) + \alpha \nabla p = \mathbf{f}_P \quad \text{in } \Omega^P \times (0, T], \quad (2.1)$$

$$(c_0 p + \alpha \operatorname{div} \mathbf{u})_t + \operatorname{div} \mathbf{w}(p) = z \quad \text{in } \Omega^P \times (0, T], \quad (2.2)$$

$$-\operatorname{div} \boldsymbol{\sigma}_E(\mathbf{u}_E) = \mathbf{f}_E \quad \text{in } \Omega^E \times (0, T], \quad (2.3)$$

where that $\mathbf{u}_P, \mathbf{u}_E$ are the solid displacements respectively in Ω^P , Ω^E and p is the fluid pressure in Ω^P . To close the model, we set the following boundary and initial conditions:

$$\mathbf{u}_P = \mathbf{0} \quad \text{on } \Gamma_d^P \times (0, T], \quad (2.4)$$

$$\hat{\boldsymbol{\sigma}}_P(\mathbf{u}_P, p) \cdot \mathbf{n}_P = \mathbf{t}_P \quad \text{on } \Gamma_t^P \times (0, T], \quad (2.5)$$

$$p = 0 \quad \text{on } \Gamma_p^P \times (0, T], \quad (2.6)$$

$$\mathbf{w}(p) \cdot \mathbf{n}_P = z_w \quad \text{on } \Gamma_f^P \times (0, T], \quad (2.7)$$

$$\mathbf{u}_E = \mathbf{0} \quad \text{on } \Gamma_d^E \times (0, T], \quad (2.8)$$

$$\boldsymbol{\sigma}_E(\mathbf{u}_E) \cdot \mathbf{n}_E = \mathbf{t}_E \quad \text{on } \Gamma_t^E \times (0, T], \quad (2.9)$$

$$\mathbf{u}(\mathbf{x}, 0) = \mathbf{u}_0(\mathbf{x}) \quad \text{in } \Omega, \quad (2.10)$$

$$p(\mathbf{x}, 0) = p_0(\mathbf{x}) \quad \text{in } \Omega^P, \quad (2.11)$$

and the following transmission conditions are introduced for interconnecting the two subdomains Ω^P and Ω^E :

$$\text{the displacement on } \Gamma \text{ is continuous:} \quad \mathbf{u}_P = \mathbf{u}_E, \quad (2.12)$$

$$\text{the normal stress on } \Gamma \text{ is continuous:} \quad -\hat{\boldsymbol{\sigma}}(\mathbf{u}_P, p) \cdot \mathbf{n}_{P \rightarrow E} = \boldsymbol{\sigma}_E(\mathbf{u}_E) \cdot \mathbf{n}_{E \rightarrow P}, \quad (2.13)$$

$$\text{there is no fluid from } \Omega^P \text{ to } \Omega^E: \quad \mathbf{w} \cdot \mathbf{n}_{P \rightarrow E} = 0, \quad (2.14)$$

where $\partial\Omega^P = \Gamma_d^P \cup \Gamma_t^P \cup \Gamma = \Gamma_p^P \cup \Gamma_f^P \cup \Gamma$ and $\partial\Omega^E = \Gamma_d^E \cup \Gamma_t^E \cup \Gamma$.

The problem (2.1)-(2.3) consists of a momentum balance in both Ω^P and Ω^E and a mass balance in Ω^P , in which $\boldsymbol{\sigma}_{\mathcal{D}}(\mathbf{u}_{\mathcal{D}})$ represents the standard stress tensor from elasticity, and in Ω^P the Darcy's law holds for the volumetric flux $\mathbf{w}(p)$ relative linearly to p . For convenience, the stress and fluid pressure term in (2.1) can be merged as the so-called total stress tensor noted by $\hat{\boldsymbol{\sigma}}_P(\mathbf{u}_P, p)$ (see Table 2.1). Parameters involved in the problem (2.1)-(2.3) are listed in Table 2.2. In the assumption that the matrix is isotropic, the permeability tensor \mathbf{K} is symmetric and uniformly positive definite, that is, for any choice of \mathbf{x} , the spectrum of $\mathbf{K}(\mathbf{x})$ has both positive lower and upper bounds.

Table 2.1: Summary of constitutive relations

Notation	Description
$\hat{\boldsymbol{\sigma}}_P(\mathbf{u}_P, p) := \boldsymbol{\sigma}_P(\mathbf{u}_P) - \alpha p \mathbf{I}$	Total stress tensor in Ω^P
$\boldsymbol{\sigma}_{\mathcal{D}}(\mathbf{u}_{\mathcal{D}}) := \lambda_{\mathcal{D}} \operatorname{div} \mathbf{u}_{\mathcal{D}} + 2\mu_{\mathcal{D}} \boldsymbol{\varepsilon}(\mathbf{u}_{\mathcal{D}})$	Effective stress tensor in $\Omega^{\mathcal{D}}$
$\mathbf{w}(p) := -\frac{\mathbf{K}}{\mu_f} (\nabla p - \rho_f \mathbf{g})$	Volumetric fluid flux in Ω^P

Table 2.2: Summary of involved parameters

Notation	Description
$\lambda_{\mathcal{D}}, \mu_{\mathcal{D}}$	Lamé constants
α	Biot-Willis constant
c_0	Fluid specific storage coefficient
\mathbf{K}	Skeleton permeability tensor
μ_f	Fluid viscosity

2.2. Multiphysics Approach. To reveal the underlying multiphysics process and overcome the locking phenomenon for the displacement variables of poroelasticity and elasticity and the pressure oscillation in computation, we set the so-called elastic pressure $\xi_{\mathcal{D}}$ and volumetric fluid content η in the following form:

$$\xi_P = \alpha p - \lambda_P \epsilon_P, \quad \xi_E = -\lambda_E \epsilon_E, \quad \eta = c_0 p + \alpha \epsilon_P, \quad \text{where} \quad \epsilon_{\mathcal{D}} := \operatorname{div} \mathbf{u}_{\mathcal{D}} \quad (2.15)$$

Since the new variables in (2.15) are linear combinations of the original variables, we can rewrite the original variables in terms of the new ones:

$$p = \kappa_1 \xi_P + \kappa_2 \eta, \quad \epsilon_P = \kappa_3 \xi_P - \kappa_1 \eta, \quad \epsilon_E = -\lambda_E^{-1} \xi_E,$$

where

$$\kappa_1 = \frac{\alpha}{\alpha^2 + c_0 \lambda_P}, \quad \kappa_2 = \frac{\lambda_P}{\alpha^2 + c_0 \lambda_P}, \quad \kappa_3 = \frac{c_0}{\alpha^2 + c_0 \lambda_P}.$$

Using the above notations, we reformulate the problem (2.1)-(2.3) into the following nearly incompressible coupled poroelasticity and elasticity model:

$$-2\mu_P \operatorname{div} \boldsymbol{\varepsilon}(\mathbf{u}_P) + \nabla \xi_P = \mathbf{f}_P \quad \text{in } \Omega^P \times (0, T], \quad (2.16)$$

$$\kappa_3 \xi_P + \operatorname{div} \mathbf{u}_P - \kappa_1 \eta = 0 \quad \text{in } \Omega^P \times (0, T], \quad (2.17)$$

$$\eta_t + \operatorname{div} \mathbf{w}(p) = z \quad \text{in } \Omega^P \times (0, T], \quad (2.18)$$

$$-2\mu_E \operatorname{div} \boldsymbol{\varepsilon}(\mathbf{u}_E) + \nabla \xi_E = \mathbf{f}_E \quad \text{in } \Omega^E \times (0, T], \quad (2.19)$$

$$\lambda_E^{-1} \xi_E + \operatorname{div} \mathbf{u}_E = 0 \quad \text{in } \Omega^E \times (0, T]. \quad (2.20)$$

Denote the total stress of the reformulated poroelasticity model by $\tilde{\boldsymbol{\sigma}}_{\mathcal{D}}(\mathbf{u}_{\mathcal{D}}, \xi_{\mathcal{D}}) := 2\mu_{\mathcal{D}} \boldsymbol{\varepsilon}(\mathbf{u}_{\mathcal{D}}) - \xi_{\mathcal{D}} \mathbf{I}$, then we can rewrite the boundary conditions as

$$\mathbf{u}_P = \mathbf{0} \quad \text{on } \Gamma_d^P \times (0, T], \quad (2.21)$$

$$\tilde{\boldsymbol{\sigma}}(\mathbf{u}_P, \xi_P) \cdot \mathbf{n}_P = \mathbf{t}_P \quad \text{on } \Gamma_t^P \times (0, T], \quad (2.22)$$

$$p = p_D \quad \text{on } \Gamma_p^P \times (0, T], \quad (2.23)$$

$$\mathbf{w}(p) \cdot \mathbf{n}_P = z_w \quad \text{on } \Gamma_f^P \times (0, T], \quad (2.24)$$

$$\mathbf{u}_E = \mathbf{0} \quad \text{on } \Gamma_d^E \times (0, T], \quad (2.25)$$

$$\tilde{\boldsymbol{\sigma}}(\mathbf{u}_E, \xi_E) \cdot \mathbf{n}_E = \mathbf{t}_E \quad \text{on } \Gamma_t^E \times (0, T], \quad (2.26)$$

and initial conditions:

$$\mathbf{u}_P(\mathbf{x}, 0) = \mathbf{u}_{P,0}(\mathbf{x}) \quad \text{in } \Omega^P, \quad (2.27)$$

$$\mathbf{u}_E(\mathbf{x}, 0) = \mathbf{u}_{E,0}(\mathbf{x}) \quad \text{in } \Omega^E, \quad (2.28)$$

$$p(\mathbf{x}, 0) = p_0(\mathbf{x}) \quad \text{in } \Omega^P, \quad (2.29)$$

$$\eta(\mathbf{x}, 0) = \eta_0(\mathbf{x}) = c_0 p_0(\mathbf{x}) - \alpha \operatorname{div} \mathbf{u}_0(\mathbf{x}) \quad \text{in } \Omega^P, \quad (2.30)$$

$$\xi_P(\mathbf{x}, 0) = \xi_{P,0}(\mathbf{x}) = \alpha p_0(\mathbf{x}) - \lambda_P \operatorname{div} \mathbf{u}_0(\mathbf{x}) \quad \text{in } \Omega^P, \quad (2.31)$$

$$\xi_E(\mathbf{x}, 0) = \xi_{E,0}(\mathbf{x}) = -\lambda_E \operatorname{div} \mathbf{u}_0(\mathbf{x}) \quad \text{in } \Omega^E, \quad (2.32)$$

and the transmission conditions:

$$\mathbf{u}_P = \mathbf{u}_E \quad \text{on } \Gamma \times (0, T], \quad (2.33)$$

$$-\tilde{\boldsymbol{\sigma}}_P(\mathbf{u}_P, \xi_P) \cdot \mathbf{n}_{P \rightarrow E} = \tilde{\boldsymbol{\sigma}}_E(\mathbf{u}_E, \xi_E) \cdot \mathbf{n}_{E \rightarrow P} \quad \text{on } \Gamma \times (0, T], \quad (2.34)$$

$$\mathbf{w}(p) \cdot \mathbf{n}_{P \rightarrow E} = 0 \quad \text{on } \Gamma \times (0, T]. \quad (2.35)$$

2.3. Variational Formulations. In this section we describe the variational formulation of the coupled poroelasticity and elasticity model with a definition of weak solutions to problems (2.1)-(2.14) and corresponding reformulated problems (2.16)-(2.35). First for any Banach or Hilbert space X , we set $\mathbf{X} := [X]^d$. We introduce the following standard notation for Sobolev spaces (see, e.g. [4]):

$$\begin{aligned}\mathbf{X}^P &= \mathbf{H}_{0d}^1(\Omega^P) := \left\{ \mathbf{v}_P \in \mathbf{H}^1(\Omega^P) : \mathbf{v}_P|_{\Gamma_d^P} = \mathbf{0} \right\}, \\ \mathbf{X}^E &= \mathbf{H}_{0d}^1(\Omega^E) := \left\{ \mathbf{v}_E \in \mathbf{H}^1(\Omega^E) : \mathbf{v}_E|_{\Gamma_d^E} = \mathbf{0} \right\}, \\ W &= H_{0p}^1(\Omega^P) := \left\{ \varphi \in H^1(\Omega^P) : \varphi|_{\Gamma_f^P} = 0 \right\},\end{aligned}$$

The inner products of $L^2(\Omega^D)$, $L^2(\Gamma_t^D)$ and $L^2(\Gamma_f^P)$ are denoted by $(\cdot, \cdot)_{\mathcal{D}}$, $\langle \cdot, \cdot \rangle_{t, \mathcal{D}}$ and $\langle \cdot, \cdot \rangle_f$, and we use the notation $\langle \cdot, \cdot \rangle_\Gamma$ to denote the inner product of $L^2(\Gamma)$:

$$\begin{aligned}(f, g)_{\mathcal{D}} &:= \int_{\Omega^D} fg \, d\mathbf{x}, & f, g \in L^2(\Omega^D) \\ \langle f, g \rangle_{t, \mathcal{D}} &:= \int_{\Gamma_t^D} fg \, ds, & f, g \in L^2(\Gamma_t^D), \\ \langle f, g \rangle_f &:= \int_{\Gamma_f^P} fg \, ds, & f, g \in L^2(\Gamma_f^P), \\ \langle f, g \rangle_\Gamma &:= \int_\Gamma fg \, ds, & f, g \in L^2(\Gamma).\end{aligned}$$

For the following description of the variational forms, let $\mathbf{u}_0 \in \mathbf{H}^1(\Omega)$, $\mathbf{f}_P \in \mathbf{L}^2(\Omega^P)$, $\mathbf{f}_E \in \mathbf{L}^2(\Omega^E)$, $\mathbf{t}_P \in \mathbf{L}^2(\Gamma_t^P)$, $\mathbf{t}^E \in \mathbf{L}^2(\Gamma_t^E)$, $p_0 \in L^2(\Omega^P)$, $h \in L^2(\Omega^P)$, $z_w \in L^2(\Gamma_f^P)$ and c_0 is assumed to be positive in Ω^P .

PROBLEM 1. Find \mathbf{u}, p with $\mathbf{u} \in L^\infty(0, T; \mathbf{X})$ and $p \in L^\infty(0, T; L^2(\Omega^P)) \cap L^2(0, T; H^1(\Omega^P))$ such that for $t \in [0, T]$ a.e.:

$$\begin{aligned}(\boldsymbol{\sigma}_P(\mathbf{u}_P), \boldsymbol{\varepsilon}(\mathbf{v}_P))_P + (\boldsymbol{\sigma}_E(\mathbf{u}_E), \boldsymbol{\varepsilon}(\mathbf{v}_E))_E - \alpha(p, \operatorname{div} \mathbf{v}_P)_P + I_\Gamma \\ = (\mathbf{f}_P, \mathbf{v}_P)_P + (\mathbf{f}_E, \mathbf{v}_E)_E + \langle \mathbf{t}_P, \mathbf{v}_P \rangle_{t, P} + \langle \mathbf{t}_E, \mathbf{v}_E \rangle_{t, E} \quad \forall \mathbf{v}_D \in \mathbf{X}^D,\end{aligned}\tag{2.36}$$

$$((c_0 p + \operatorname{div} \mathbf{u}_P)_t, \varphi)_P + \frac{1}{\mu_f} (\mathbf{K}(\nabla p - \rho_f \mathbf{g}), \nabla \varphi) = (z, \varphi)_P + \langle z_w, \varphi \rangle_f \quad \forall \varphi \in W,\tag{2.37}$$

$$\mathbf{u}(0) = \mathbf{u}_0 \text{ in } \Omega, \quad p(0) = p_0 \text{ in } \Omega^P,\tag{2.38}$$

where the interface term I_Γ takes the form:

$$I_\Gamma = -\langle \hat{\boldsymbol{\sigma}}(\mathbf{u}_P, p) \cdot \mathbf{n}_{P \rightarrow E}, \mathbf{v}_P \rangle_\Gamma - \langle \boldsymbol{\sigma}_E(\mathbf{u}_E) \cdot \mathbf{n}_{E \rightarrow P}, \mathbf{v}_E \rangle_\Gamma.$$

According to the normal stress continuity (2.13), we define the Lagrange multiplier:

$$\boldsymbol{\lambda} = -\hat{\boldsymbol{\sigma}}(\mathbf{u}_P, p) \cdot \mathbf{n}_{P \rightarrow E} = \boldsymbol{\sigma}_E(\mathbf{u}_E) \cdot \mathbf{n}_{E \rightarrow P},\tag{2.39}$$

then the interface term in Problem 1 can be written in

$$I_\Gamma = b_\Gamma(\mathbf{v}_P, \mathbf{v}_E; \boldsymbol{\lambda}),\tag{2.40}$$

where

$$b_\Gamma(\mathbf{v}_P, \mathbf{v}_E; \boldsymbol{\mu}) = \langle \mathbf{v}_P - \mathbf{v}_E, \boldsymbol{\mu} \rangle_\Gamma.$$

To guarantee the well-posedness of b_Γ , we require the following space[19]:

$$\boldsymbol{\lambda} \in \boldsymbol{\Lambda} := \mathbf{H}_{00}^{-1/2}(\Gamma),$$

which is the dual space of $\mathbf{H}_{00}^{1/2}(\Gamma)$.

Next, we prescribe the variational formulation of the problem (2.16)-(2.35). For convenience, we introduce the following bilinear forms:

$$a_{\mathcal{D}}(\mathbf{u}_{\mathcal{D}}, \mathbf{v}_{\mathcal{D}}) = 2\mu_{\mathcal{D}}(\varepsilon(\mathbf{u}_{\mathcal{D}}), \varepsilon(\mathbf{v}_{\mathcal{D}}))_{\mathcal{D}}, \quad (2.41)$$

$$b_{\mathcal{D}}(\mathbf{v}_{\mathcal{D}}, \xi_{\mathcal{D}}) = -(\xi_{\mathcal{D}}, \operatorname{div} \mathbf{v}_{\mathcal{D}})_{\mathcal{D}}, \quad (2.42)$$

$$a_f(p, q) = \frac{1}{\mu_f} (\mathbf{K} \nabla p, \nabla q)_P. \quad (2.43)$$

PROBLEM 2. Find \mathbf{u}, ξ, η, p for $T > 0$ with $\mathbf{u} \in L^\infty(0, T; \mathbf{X})$, $\xi \in L^2(0, T; L^2(\Omega))$, $\eta \in L^\infty(0, T; L^2(\Omega)) \cap H^1(0, T; W')$ and $p \in L^\infty(0, T; L^2(\Omega)) \cap L^2(0, T; W)$ for $t \in [0, T]$ such that

$$a_P(\mathbf{u}_P, \mathbf{v}_P) + b_P(\mathbf{v}_P, \xi_P) = (\mathbf{f}_P, \mathbf{v}_P)_P + \langle \mathbf{t}_P, \mathbf{v}_P \rangle_{t,P} + \langle \boldsymbol{\lambda}, \mathbf{v}_P \rangle_\Gamma \quad \forall \mathbf{v}_P \in \mathbf{X}^P, \quad (2.44)$$

$$b_P(\mathbf{u}_P, \zeta_P) - \kappa_3(\xi_P, \zeta_P) + \kappa_1(\eta, \zeta_P)_P = 0 \quad \forall \zeta_P \in L^2(\Omega^P), \quad (2.45)$$

$$\kappa_1(\xi_P, \psi)_P + \kappa_2(\eta, \psi)_P - (p, \psi)_P = 0 \quad \forall \psi \in L^2(\Omega^P), \quad (2.46)$$

$$(\eta_t, q) + a_f(p, q) = (z, q)_P + \langle z_w, q \rangle_f + \frac{\rho_f}{\mu_f} (\mathbf{K} \mathbf{g}, \nabla q)_P \quad \forall q \in W, \quad (2.47)$$

$$a_E(\mathbf{u}_E, \mathbf{v}_E) + b_E(\mathbf{v}_E, \xi_E) = (\mathbf{f}_E, \mathbf{v}_E)_E + \langle \mathbf{t}_E, \mathbf{v}_E \rangle_{t,E} - \langle \boldsymbol{\lambda}, \mathbf{v}_E \rangle_\Gamma \quad \forall \mathbf{v}_E \in \mathbf{X}^E, \quad (2.48)$$

$$b_E(\mathbf{u}_E, \zeta_E) - \lambda_E^{-1}(\xi_E, \zeta_E)_E = 0 \quad \forall \zeta_E \in L^2(\Omega^E), \quad (2.49)$$

$$\langle \mathbf{u}_P - \mathbf{u}_E, \boldsymbol{\mu} \rangle_\Gamma = 0 \quad \forall \boldsymbol{\mu} \in \boldsymbol{\Lambda}, \quad (2.50)$$

$$\mathbf{u}(0) = \mathbf{u}_0, \quad p_h(0) = p_0, \quad (2.51)$$

$$\xi(0) = \xi_0, \quad \eta(0) = \eta_0. \quad (2.52)$$

2.4. Semi-discrete Scheme. Let $\mathcal{T}_h^{\mathcal{D}}(I = P, E)$ be a suitable triangulation or rectangular partition for subdomain $\Omega^{\mathcal{D}}$, where $\overline{\Omega^{\mathcal{D}}} = \bigcup_{K \in \mathcal{T}_h^{\mathcal{D}}} \overline{K}$, and let $(\mathbf{X}_h^{\mathcal{D}}, M_h^{\mathcal{D}})$ be the space of suitable mixed finite element functions pair. We can naturally note the corresponding triangulation and finite element pair from the above definitions by $\mathcal{T}_h = \mathcal{T}_h^P \cup \mathcal{T}_h^E$, $\mathbf{X}_h = \mathbf{X}_h^P \oplus \mathbf{X}_h^E$ and $M_h = M_h^P \oplus M_h^E$. Note that finite element space W_h for the fluid pressure p and volumetric fluid content η in Ω^P can be chosen independently, any choice that $W_h \supset M_h^P$ is acceptable. In this section we consider the convenient choice that $W_h = M_h^P$. In addition, let $\boldsymbol{\Lambda}_h$ denotes the finite element space of the Lagrange multiplier $\boldsymbol{\lambda}$. In this paper, we adopt \mathbf{P}_k - P_l element $(\mathbf{X}_h^{\mathcal{D}}, M_h^{\mathcal{D}})$ for $\mathbf{u}_{\mathcal{D}}, \xi_{\mathcal{D}}$:

$$\begin{aligned} \mathbf{X}_h^{\mathcal{D}} &:= \left\{ \mathbf{v}_h \in \mathbf{C}^0(\overline{\Omega^{\mathcal{D}}}) : \mathbf{v}_{\mathcal{D},h}|_K \in \mathbf{P}_k(K) \quad \forall K \in \mathcal{T}_h^{\mathcal{D}} \right\}, \\ M_h^{\mathcal{D}} &:= \left\{ \varphi_h \in C^0(\overline{\Omega^{\mathcal{D}}}) : \varphi_{\mathcal{D},h}|_K \in P_l(K) \quad \forall K \in \mathcal{T}_h^{\mathcal{D}} \right\}. \end{aligned}$$

where k, l will be specifically given in the test cases. In the latter description, we will always use $(\mathbf{P}_k$ - P_l - P_l - P_l , \mathbf{P}_k - P_l) to denote that we use \mathbf{P}_k - P_l - P_l - P_l finite element space for poroelasticity and \mathbf{P}_k - P_l finite element space for elasticity. Now, we give the finite element discretized variational formulation in the following:

PROBLEM 3. Find $\mathbf{u}_h, \xi_h, \eta_h, p_h$ for $T > 0$ with $\mathbf{u}_h \in L^\infty(0, T; \mathbf{X}_h)$, $\xi_h \in L^\infty(0, T; M_h)$, $\eta_h \in L^\infty(0, T; M_h^P) \cap H^1(0, T; W_h')$ and $p_h \in L^\infty(0, T; M_h) \cap L^2(0, T; W_h)$ for $t \in [0, T]$ such that

$$a_P(\mathbf{u}_{P,h}, \mathbf{v}_{P,h}) + b_P(\mathbf{v}_{P,h}, \xi_{P,h}) = (\mathbf{f}_P, \mathbf{v}_{P,h})_P + \langle \mathbf{t}_P, \mathbf{v}_{P,h} \rangle_{t,P} - \langle \boldsymbol{\lambda}_h, \mathbf{v}_{P,h} \rangle_\Gamma \quad \forall \mathbf{v}_{P,h} \in \mathbf{X}_h^P, \quad (2.53)$$

$$b_P(\mathbf{u}_{P,h}, \zeta_{P,h}) - \kappa_3(\xi_{P,h}, \zeta_{P,h})_P + \kappa_1(\eta_h, \zeta_{P,h})_P = 0 \quad \forall \zeta_{P,h} \in M_h^P, \quad (2.54)$$

$$\kappa_1(\xi_{P,h}, \psi_h)_P + \kappa_2(\eta_h, \psi_h)_P - (p_h, \psi_h) = 0 \quad \forall \psi_h \in W_h \quad (2.55)$$

$$(\eta_{h,t}, q_h)_P + a_f(p_h, q_h) = (z, q_h)_P + \langle z_w, q_h \rangle_f + \frac{\rho_f}{\mu_f} (\mathbf{K} \mathbf{g}, \nabla q_h)_P \quad \forall q_h \in W_h, \quad (2.56)$$

$$a_E(\mathbf{u}_{E,h}, \mathbf{v}_{E,h}) + b_E(\mathbf{v}_{E,h}, \xi_{E,h}) = (\mathbf{f}_E, \mathbf{v}_{E,h})_E + \langle \mathbf{t}_E, \mathbf{v}_{E,h} \rangle_{t,E} + \langle \boldsymbol{\lambda}_h, \mathbf{v}_{E,h} \rangle_\Gamma \quad \forall \mathbf{v}_{E,h} \in \mathbf{X}_h^E, \quad (2.57)$$

$$b_E(\mathbf{u}_{E,h}, \zeta_{E,h}) - \lambda_E^{-1}(\xi_{E,h}, \zeta_{E,h})_E = 0 \quad \forall \zeta_{E,h} \in M_h^E, \quad (2.58)$$

$$\langle \mathbf{u}_{P,h} - \mathbf{u}_{E,h}, \boldsymbol{\mu}_h \rangle_\Gamma = 0 \quad \forall \boldsymbol{\mu}_h \in \boldsymbol{\Lambda}_h, \quad (2.59)$$

$$\mathbf{u}_h(0) = \mathbf{u}_{0,h}, \quad p_h(0) = p_{0,h}, \quad (2.60)$$

$$\xi_h(0) = \xi_{0,h}, \quad \eta_h(0) = \eta_{0,h}. \quad (2.61)$$

where $\mathbf{u}_{0,h}, p_{0,h}, \xi_{0,h}$ and $\eta_{0,h}$ are the projections of the initial conditions respectively.

REMARK 2.1. In practical actuality, we do not need to choose finite element spaces that the inf-sup condition holds, that is, the space \mathbf{X}_h^D and M_h^D with $k > l$, which can be demonstrated by the proof of existence and uniqueness of solutions of the following matrix-vector forms in Theorem 3.1.

2.5. Fully-discrete Scheme. In this section, we will describe the fully-discrete scheme by the backward Euler method for time discretization. To do that, we assume that the time interval $[0, T]$ is divided uniformly into N segments by setting $t_n = n\tau$, where $\tau = T/N$ is the time step size and $n = 0, 1, \dots, N$, and let $\mathcal{G}^n := \mathcal{G}(t_n)$, where \mathcal{G} denotes any variable.

We give the following fully discretized variational formulation in the following:

PROBLEM 4. Find $\mathbf{u}_h^n, \xi_h^n, \eta_h^n, p_h^n$ with $\mathbf{u}_h^n \in \mathbf{X}_h$, $\xi_h^n \in M_h$, $\eta_h^n \in W_h$ and $p_h^n \in W_h$ for $n = 1, \dots, N$ such that:

$$a_P(\mathbf{u}_{P,h}^n, \mathbf{v}_{P,h}) + b_P(\mathbf{v}_{P,h}, \xi_{P,h}^n) = (\mathbf{f}_P(t_n), \mathbf{v}_{P,h})_P + \langle \mathbf{t}_P(t_n), \mathbf{v}_{P,h} \rangle_{t,P} - \langle \boldsymbol{\lambda}_h^n, \mathbf{v}_{P,h} \rangle_\Gamma \quad \forall \mathbf{v}_{P,h} \in \mathbf{X}_h^P, \quad (2.62)$$

$$b(\mathbf{u}_{P,h}^n, \zeta_{P,h}) - \kappa_3(\xi_{P,h}^n, \zeta_{P,h})_P + \kappa_1(\eta_h^n, \zeta_{P,h})_P = 0 \quad \forall \zeta_{P,h} \in M_h^P, \quad (2.63)$$

$$\kappa_1(\xi_{P,h}^n, \psi_h)_P + \kappa_2(\eta_h^n, \psi_h)_P - (p_h^n, \psi_h) = 0 \quad \forall \psi_h \in W_h \quad (2.64)$$

$$(\partial_t \eta_h^n, q_h)_P + a_f(p_h^n, q_h) = (z(t_n), q_h)_P + \langle z_w(t_n), q_h \rangle_f + \frac{\rho_f}{\mu_f}(\mathbf{K}\mathbf{g}, \nabla q_h)_P \quad \forall q_h \in W_h, \quad (2.65)$$

$$a_E(\mathbf{u}_{E,h}^n, \mathbf{v}_{E,h}) + b_E(\mathbf{v}_{E,h}, \xi_{E,h}^n) = (\mathbf{f}_P(t_n), \mathbf{v}_{E,h})_E + \langle \mathbf{t}_E(t_n), \mathbf{v}_{E,h} \rangle_{t,E} + \langle \boldsymbol{\lambda}_h^n, \mathbf{v}_{E,h} \rangle_\Gamma \quad \forall \mathbf{v}_{E,h} \in \mathbf{X}_h^E, \quad (2.66)$$

$$b_E(\mathbf{u}_{E,h}^n, \zeta_{E,h}) - \lambda_E^{-1}(\xi_{E,h}^n, \zeta_{E,h})_E = 0 \quad \forall \zeta_{E,h} \in M_h^E, \quad (2.67)$$

$$\langle \mathbf{u}_{P,h}^n - \mathbf{u}_{E,h}^n, \boldsymbol{\mu}_h \rangle_\Gamma = 0 \quad \forall \boldsymbol{\mu}_h \in \boldsymbol{\Lambda}_h, \quad (2.68)$$

$$\mathbf{u}_h^0 = \mathbf{u}_{0,h}, \quad p_h^0 = p_{0,h}, \quad (2.69)$$

$$\xi_h^0 = \xi_{0,h}, \quad \eta_h^0 = \eta_{0,h}. \quad (2.70)$$

where the backward difference quotient $\partial_t \eta_h^n$ is defined as

$$\partial_t \eta_h^n = \frac{\eta_h^n - \eta_h^{n-1}}{\tau}, \quad (2.71)$$

and where $\mathbf{u}_{0,h}, p_{0,h}, \xi_{0,h}$ and $\eta_{0,h}$ are the projections of the initial conditions respectively.

Applying (2.71) to (2.65) yields the following:

$$-(\eta_h^n, q_h)_P - \tau a_f(p_h^n, q_h) = -(\eta_h^{n-1} + \tau z(t_n), q_h)_P - \tau \langle z_w(t_n), q_h \rangle_f - \frac{\tau \rho_f}{\mu_f}(\mathbf{K}\mathbf{g}, \nabla q_h)_P, \quad \forall q_h \in W_h. \quad (2.72)$$

which is the finite element formulation of an elliptic equation.

We now construct the linear systems at each time step. Let $\mathbf{X}_h^D = \text{span}\{\boldsymbol{\theta}_{\mathcal{D},i}\}_{i=1}^{N_{\mathbf{u}}^D}$, $M_h^D = \text{span}\{\phi_{\mathcal{D},i}\}_{i=1}^{N_{\xi}^D}$, $W_h = \text{span}\{\phi_i\}_{i=1}^{N_p}$ and $\boldsymbol{\Lambda}_h = \text{span}\{\mathbf{v}_i\}_{i=1}^{N_{\lambda}}$, where $N_{\mathbf{u}}^D$, N_{ξ}^D , N_p and N_{λ} are the degrees of freedoms to \mathbf{X}_h^D , M_h^D , W_h and $\boldsymbol{\Lambda}_h$ respectively. According the settings of finite element space for each variables, we write $\mathbf{u}_{\mathcal{D},h}(t) = \sum_{i=1}^{N_{\mathbf{u}}^D} \mathbf{u}_{\mathcal{D},i}(t) \boldsymbol{\theta}_{\mathcal{D},i}$, $\xi_{\mathcal{D},h}(t) = \sum_{i=1}^{N_{\xi}^D} \xi_{\mathcal{D},i}(t) \phi_{\mathcal{D},i}$, $\eta_h(t) = \sum_{i=1}^{N_p} \eta_i(t) \phi_{P,i}$, $p_h(t) = \sum_{i=1}^{N_p} p_i(t) \phi_{P,i}$ and $\boldsymbol{\lambda}_h = \sum_{i=1}^{N_{\lambda}} \boldsymbol{\lambda}_i(t) \mathbf{v}_i$. The fully-discretized system deriving from Problem 4 can be written in the following matrix-vector form: for each time step

$n = 1, 2, \dots, N$, find $\mathbf{u}_{D,h}^n$, $\xi_{D,h}^n$, η_h^n and p_h^n such that

$$\begin{bmatrix} \mathcal{A}_P & \mathcal{B}_P^T & \mathcal{O} & \mathcal{O} & \mathcal{O} & \mathcal{O} & \mathcal{H}_P^T \\ \mathcal{B}_P & -\kappa_3 \mathcal{R}_P & \kappa_1 \mathcal{R}_P & \mathcal{O} & \mathcal{O} & \mathcal{O} & \mathcal{O} \\ \mathcal{O} & \kappa_1 \mathcal{R}_P & \kappa_2 \mathcal{R}_P & -\mathcal{R}_P & \mathcal{O} & \mathcal{O} & \mathcal{O} \\ \mathcal{O} & \mathcal{O} & -\mathcal{R}_P & -\tau \mathcal{A}_f & \mathcal{O} & \mathcal{O} & \mathcal{O} \\ \mathcal{O} & \mathcal{O} & \mathcal{O} & \mathcal{O} & \mathcal{A}_E & \mathcal{B}_E^T & -\mathcal{H}_E^T \\ \mathcal{O} & \mathcal{O} & \mathcal{O} & \mathcal{O} & \mathcal{B}_E & -\lambda_E^{-1} \mathcal{R}_E & \mathcal{O} \\ \mathcal{H}_P & \mathcal{O} & \mathcal{O} & \mathcal{O} & -\mathcal{H}_E & \mathcal{O} & \mathcal{O} \end{bmatrix} \begin{bmatrix} \mathbf{u}_{P,h}^n \\ \xi_{P,h}^n \\ \eta_h^n \\ p_h^n \\ \mathbf{u}_{E,h}^n \\ \xi_{E,h}^n \\ \lambda_h^n \end{bmatrix} = \begin{bmatrix} \mathcal{F}_P^n \\ \mathcal{O} \\ \mathcal{O} \\ -\mathcal{R}_P \eta_h^{n-1} - \tau \mathcal{Z}^n \\ \mathcal{F}_E^n \\ \mathcal{O} \\ \mathcal{O} \end{bmatrix}, \quad (2.73)$$

where the corresponding representations of the above block matrices and vectors are

$$\begin{aligned} [\mathcal{A}_P]_{ij} &= a_P(\boldsymbol{\theta}_{P,i}, \boldsymbol{\theta}_{P,j}), & [\mathcal{A}_E]_{ij} &= a_E(\boldsymbol{\theta}_{E,i}, \boldsymbol{\theta}_{E,j}), \\ [\mathcal{B}_P]_{ij} &= b_P(\boldsymbol{\theta}_{P,j}, \phi_{P,i}), & [\mathcal{B}_E]_{ij} &= b_E(\boldsymbol{\theta}_{E,j}, \phi_{E,i}), \\ [\mathcal{H}_P]_{ij} &= \langle \boldsymbol{\theta}_{P,j}, \mathbf{v}_i \rangle_\Gamma, & [\mathcal{H}_E]_{ij} &= \langle \boldsymbol{\theta}_{E,j}, \mathbf{v}_i \rangle_\Gamma, \\ [\mathcal{R}_P]_{ij} &= (\phi_{P,i}, \phi_{P,j}), & [\mathcal{R}_E]_{ij} &= (\phi_{E,i}, \phi_{E,j}), \\ [\mathcal{F}_P]_i &= (\mathbf{f}_P(t_n), \boldsymbol{\theta}_{P,i}) + \langle \mathbf{t}_P(t_n), \boldsymbol{\theta}_{P,i} \rangle_{t,P}, & [\mathcal{F}_E]_i &= (f_E(t_n), \boldsymbol{\theta}_{E,i}) + \langle \mathbf{t}_E(t_n), \boldsymbol{\theta}_{E,i} \rangle, \end{aligned}$$

$$[\mathcal{Z}^n]_i = (z(t_n), \phi_{P,i})_P + \langle z_w(t_n), \phi_{P,i} \rangle_f + \frac{\rho_f}{\mu_f} (\mathbf{K} \mathbf{g}, \nabla \phi_{P,i})_P.$$

REMARK 2.2. The fully-discretized scheme described in Problem 4 is not optimal for parallel solving. Assume that the degree of freedoms for \mathcal{T}_P and \mathcal{T}_E are the same, since the reformulated poroelasticity subproblem (2.62)-(2.65) has extra two variables η , p compared to the nearly-incompressible elasticity subproblem (2.66)-(2.67), the computational cost for solving the poroelasticity subproblem is much higher than that of the elasticity subproblem, which leads to load imbalance in parallel computing. To overcome this issue, we need to adopt the explicit time discretization for the equation of η , p in (2.56) in order to decouple the momentum balance equations (2.53)-(2.54) and the mass balance equation (2.55)-(2.56). However, classical linear explicit schemes may lead to too strict stability condition, which forces us to choose an unacceptably small time step size. To this end, we can consider the exponential integrator[12] for a accuracy-preserving decoupling.

3. The FETI Method. In this section we consider implementing the FETI method to the coupled poroelasticity and elasticity problem. The target of discussing the FETI algorithm is to find the displacement on the interface $\mathbf{u}|_\Gamma$ such that the poroelasticity and elasticity subproblems in their corresponding subdomains can be solved independently as generalized single-region problems, which has the potential for parallelization. To see this, we first reduce the saddle point system (2.73) to a smaller one for solving interface displacement $\mathbf{u}_h^n|_\Gamma$ and Lagrange multiplier λ_h^n only. For the reduced system, since the difficulty for explicitly showing the stiffness matrix, we consider a preconditioned conjugate gradient (PCG) method with the FETI Dirichlet preconditioner(cf. [19]).

3.1. The FETI Algorithm and Preconditioner. Before starting the description, we first reorder some variables so that each subproblem has the form of saddle-point system. We set

$$\mathcal{U}_{P,h}(t) = \begin{bmatrix} \mathbf{u}_{P,h}(t) \\ \eta_h(t) \end{bmatrix}, \quad \mathcal{U}_{E,h}(t) = \mathbf{u}_{E,h}(t), \quad \mathcal{P}_{P,h}(t) = \begin{bmatrix} \xi_{P,h}(t) \\ p_h(t) \end{bmatrix}, \quad \mathcal{P}_{E,h}(t) = \xi_{E,h}(t),$$

, and then we rewrite (2.73) in the following form:

$$\mathcal{K} \begin{bmatrix} \mathcal{U}_{P,h}^n & \mathcal{P}_{P,h}^n & \mathcal{U}_{E,h}^n & \mathcal{P}_{E,h}^n & \lambda_h^n \end{bmatrix}^T = \begin{bmatrix} \mathcal{F}_{P,*}^n & \mathcal{Z}_*^n & \mathcal{F}_{E,*}^n & \mathcal{O} & \mathcal{O} \end{bmatrix}^T, \quad (3.1)$$

where

$$\mathcal{K} = \begin{bmatrix} \mathcal{A}_P^* & (\mathcal{B}_P^*)^T & \mathcal{O} & \mathcal{O} & (\mathcal{H}_P^*)^T \\ \mathcal{B}_P^* & -\mathcal{C}_P^* & \mathcal{O} & \mathcal{O} & \mathcal{O} \\ \mathcal{O} & \mathcal{O} & \mathcal{A}_E & \mathcal{B}_E^T & (\mathcal{H}_E^*)^T \\ \mathcal{O} & \mathcal{O} & \mathcal{B}_E & -\lambda_E^{-1} \mathcal{R}_E & \mathcal{O} \\ \mathcal{H}_P^* & \mathcal{O} & \mathcal{H}_E^* & \mathcal{O} & \mathcal{O} \end{bmatrix}, \quad \mathcal{F}_{P,*}^n = \begin{bmatrix} \mathcal{F}_P^n \\ \mathcal{O} \end{bmatrix}, \quad \mathcal{Z}_*^n = \begin{bmatrix} \mathcal{O} \\ -\mathcal{R}_P \eta_h^{n-1} - \tau \mathcal{Z}^n \end{bmatrix}, \quad \mathcal{F}_{E,*}^n = \begin{bmatrix} \mathcal{F}_E^n \\ \mathcal{O} \end{bmatrix},$$

and where

$$\mathcal{A}_P^* = \begin{bmatrix} \mathcal{A}_P & \mathcal{O} \\ \mathcal{O} & \kappa_2 \mathcal{R}_P \end{bmatrix}, \quad \mathcal{B}_P^* = \begin{bmatrix} \mathcal{B}_P & \kappa_1 \mathcal{R}_P \\ \mathcal{O} & -\mathcal{R}_P \end{bmatrix}, \quad \mathcal{C}_P^* = \begin{bmatrix} \kappa_3 \mathcal{R}_P & \mathcal{O} \\ \mathcal{O} & \mathcal{A}_f \end{bmatrix}, \quad \mathcal{H}_P^* = [\mathcal{H}_P \quad \mathcal{O}].$$

We first reorder the vector of degrees of freedom $\mathcal{U}_{\mathcal{D},h}^n$ as $(\mathcal{U}_{\mathcal{D},h,I}^n, \mathcal{U}_{\mathcal{D},h,B}^n)^T$ and corresponding load vectors as $\mathcal{F}_{\mathcal{D}}^n = (\mathcal{F}_{\mathcal{D},I}^n, \mathcal{F}_{\mathcal{D},B}^n)^T$, which yields from (3.1) the following reordered system:

$$\begin{bmatrix} \mathcal{A}_{P,II}^* & (\mathcal{B}_{P,I}^*)^T & (\mathcal{A}_{P,IB}^*)^T & \mathcal{O} & \mathcal{O} & \mathcal{O} & \mathcal{O} \\ \mathcal{B}_{P,I}^* & -\mathcal{C}_P^* & (\mathcal{B}_{P,B}^*)^T & \mathcal{O} & \mathcal{O} & \mathcal{O} & \mathcal{O} \\ \mathcal{A}_{P,IB}^* & \mathcal{B}_{P,B}^* & \mathcal{A}_{P,BB}^* & \mathcal{O} & \mathcal{O} & \mathcal{O} & \mathcal{H}_P^T \\ \mathcal{O} & \mathcal{O} & \mathcal{O} & \mathcal{A}_{E,II} & \mathcal{B}_{E,I}^T & \mathcal{A}_{E,IB}^T & \mathcal{O} \\ \mathcal{O} & \mathcal{O} & \mathcal{O} & \mathcal{B}_{E,I} & -\mathcal{C}_E & \mathcal{B}_{E,B}^T & \mathcal{O} \\ \mathcal{O} & \mathcal{O} & \mathcal{O} & \mathcal{A}_{E,IB} & \mathcal{B}_{E,B} & \mathcal{A}_{E,BB} & \mathcal{H}_E^T \\ \mathcal{O} & \mathcal{O} & \mathcal{H}_P & \mathcal{O} & \mathcal{O} & \mathcal{H}_E & \mathcal{O} \end{bmatrix} \begin{bmatrix} \mathcal{U}_{P,h,I}^n \\ \mathcal{P}_{P,h}^n \\ \mathcal{U}_{P,h,B}^n \\ \mathcal{U}_{E,h,I}^n \\ \mathcal{P}_{E,h}^n \\ \mathcal{U}_{E,h,B}^n \\ \boldsymbol{\lambda}_h^n \end{bmatrix} = \begin{bmatrix} \mathcal{F}_{P,I}^n \\ \mathcal{Z}_*^n \\ \mathcal{F}_{P,B}^n \\ \mathcal{F}_{E,I}^n \\ \mathcal{O} \\ \mathcal{F}_{E,B}^n \\ \mathcal{O} \end{bmatrix}. \quad (3.2)$$

Substituting this expression into the second block row of (3.2) yields a reduced saddle point system for determining $\mathcal{U}_{\mathcal{D},h,B}^n$, that is, the reduced saddle point system:

$$\begin{bmatrix} \mathcal{S}_P & \mathcal{O} & \mathcal{H}_P^T \\ \mathcal{O} & \mathcal{S}_E & \mathcal{H}_E^T \\ \mathcal{H}_P & \mathcal{H}_E & \mathcal{O} \end{bmatrix} \begin{bmatrix} \mathcal{U}_{P,h,B}^n \\ \mathcal{U}_{E,h,B}^n \\ \boldsymbol{\lambda}_h^n \end{bmatrix} = \begin{bmatrix} \tilde{\mathcal{F}}_{P,B}^n \\ \tilde{\mathcal{F}}_{E,B}^n \\ \mathcal{O} \end{bmatrix}, \quad (3.3)$$

where

$$\begin{aligned} \mathcal{S}_P &= \mathcal{A}_{P,BB}^* - [\mathcal{A}_{P,IB}^* \quad \mathcal{B}_{P,B}^*] \begin{bmatrix} \mathcal{A}_{P,II}^* & (\mathcal{B}_{P,I}^*)^T \\ \mathcal{B}_{P,I}^* & -\mathcal{C}_P^* \end{bmatrix}^{-1} \begin{bmatrix} (\mathcal{A}_{P,IB}^*)^T \\ (\mathcal{B}_{P,B}^*)^T \end{bmatrix}, \\ \mathcal{S}_E &= \mathcal{A}_{E,BB} - [\mathcal{A}_{E,IB} \quad \mathcal{B}_{E,B}] \begin{bmatrix} \mathcal{A}_{E,II} & \mathcal{B}_{E,I}^T \\ \mathcal{B}_{E,I} & -\mathcal{C}_E \end{bmatrix}^{-1} \begin{bmatrix} \mathcal{A}_{E,IB}^T \\ \mathcal{B}_{E,B}^T \end{bmatrix}, \end{aligned}$$

and

$$\begin{aligned} \tilde{\mathcal{F}}_{P,B}^n &= \tilde{\mathcal{F}}_{P,B}^n - \mathcal{A}_{P,BB} - [\mathcal{A}_{P,IB} \quad \mathcal{B}_{P,B}] \begin{bmatrix} \mathcal{F}_{P,I}^n \\ \mathcal{Z}_*^n \end{bmatrix}, \\ \tilde{\mathcal{F}}_{E,B}^n &= \tilde{\mathcal{F}}_{E,B}^n - \mathcal{A}_{E,BB} - [\mathcal{A}_{E,IB} \quad \mathcal{B}_{E,B}] \begin{bmatrix} \mathcal{F}_{E,I}^n \\ \mathcal{O} \end{bmatrix}. \end{aligned}$$

We now describe the existence and uniqueness of solutions of (3.2) in the following.

THEOREM 3.1. *The matrix-vector form (2.73), reordered into (3.2), is uniquely solvable.*

Proof. In actuality, according to the reduction from (3.2) to (3.3), the stiffness matrix in (3.2) is transformed into the following diagonal form:

$$\text{diag} \left\{ \begin{bmatrix} \mathcal{A}_{P,II}^* & (\mathcal{B}_{P,I}^*)^* \\ \mathcal{B}_{P,I}^* & -\mathcal{C}_P^* \end{bmatrix}, \begin{bmatrix} \mathcal{A}_{E,II} & \mathcal{B}_{E,I}^T \\ \mathcal{B}_{E,I} & -\mathcal{C}_E \end{bmatrix}, \begin{bmatrix} \mathcal{S}_P & \mathcal{O} & \mathcal{H}_P^T \\ \mathcal{O} & \mathcal{S}_E & \mathcal{H}_E^T \\ \mathcal{H}_P & \mathcal{H}_E & \mathcal{O} \end{bmatrix} \right\}.$$

We need only to prove respectively that the above three diagonal blocks are all non-singular and then the correspondingly subequations are all uniquely solvable.

First we prove that the Schur complement $\mathcal{S}_P, \mathcal{S}_E$ are both symmetric and positive definite. From the Sylvester's law of inertia, the number of positive, zero and negative eigenvalues do not change through elementary transformations, thus we can verify that the Schur complement \mathcal{S}_P and \mathcal{S}_E are symmetric and positive definite.

Then we need only to prove that the reduced system (3.3), which is a standard saddle point system, is uniquely solvable. Since the block diagonal diag $(\mathcal{S}_P, \mathcal{S}_E)$ is symmetric and positive definite and $[\mathcal{H}_P, \mathcal{H}_E]$ is surjective, the reduced system (3.3) is uniquely solvable according to Corollary 3.2.1 in [4].

Once we have solved the interface displacement $\mathcal{U}_{\mathcal{D},h,B}$ and Lagrange multiplier λ_h^n , the solution of (2.73) can be obtained by solving (3.3) for $\mathcal{U}_{P,h,B}^n$, $\mathcal{U}_{E,h,B}^n$, λ_h^n and then consequently solve

$$\begin{bmatrix} \mathcal{A}_{P,II}^* & (\mathcal{B}_{P,I}^*)^T \\ \mathcal{B}_{P,I}^* & \mathcal{C}_P^* \end{bmatrix} \begin{bmatrix} \mathcal{U}_{P,h,I}^n \\ \mathcal{P}_{P,h}^n \end{bmatrix} = \begin{bmatrix} \mathcal{F}_{P,I}^n \\ \mathcal{I}_\tau \mathcal{Z}^n \end{bmatrix} - \begin{bmatrix} (\mathcal{A}_{P,IB}^*)^T \\ (\mathcal{B}_{P,B}^*)^T \end{bmatrix} \mathcal{U}_{P,h,B}^n - \mathcal{H}_{P,B}^T \lambda_h^n,$$

$$\begin{bmatrix} \mathcal{A}_{E,II} & \mathcal{B}_{E,I}^T \\ \mathcal{B}_{E,I} & -\mathcal{C}_E \end{bmatrix} \begin{bmatrix} \mathcal{U}_{E,h,I}^n \\ \mathcal{P}_{E,h}^n \end{bmatrix} = \begin{bmatrix} \mathcal{F}_{E,I}^n \\ \mathcal{O} \end{bmatrix} - \begin{bmatrix} \mathcal{A}_{E,IB}^T \\ \mathcal{B}_{E,B}^T \end{bmatrix} \mathcal{U}_{E,h,B}^n - \mathcal{H}_{E,B}^T \lambda_h^n$$

for $\mathcal{U}_{P,h,I}^n$ and $\mathcal{U}_{E,h,I}^n$. The existence and uniqueness of solutions of the above two subsystems can be easily proved by Proposition 3.3.1 in [4]. \square

REMARK 3.1. The proof of Theorem 3.1 shows that $\mathcal{B}_{\mathcal{D},I}$ need not be surjective. Corresponding to the choices of finite element spaces, there is no need to satisfy the inf-sup condition, which means that the lowest-order finite element spaces can be chosen without vanishing the existence and uniqueness of solutions.

By eliminating $\mathcal{H}_{P,B}$, $\mathcal{H}_{E,B}$ in the third block row, we can obtain the Schur complement system of (3.3):

$$\mathcal{K}_S \lambda_h^n = \mathcal{F}_S^n, \quad (3.4)$$

where

$$\begin{aligned} \mathcal{K}_S &= \mathcal{H}_{P,B} \mathcal{S}_P^{-1} \mathcal{H}_{P,B}^T + \mathcal{H}_{E,B} \mathcal{S}_E^{-1} \mathcal{H}_{E,B}^T \\ \mathcal{F}_S^n &= \mathcal{H}_{P,B} \mathcal{S}_P^{-1} \mathcal{H}_{P,B}^T \tilde{\mathcal{F}}_{P,B}^n + \mathcal{H}_{E,B} \mathcal{S}_E^{-1} \tilde{\mathcal{F}}_{E,B}^n. \end{aligned}$$

Since \mathcal{K}_S , \mathcal{F}_S can neither be expressed explicitly, we consider a PCG method for solving (3.4). In this paper, we consider the FETI Dirichlet preconditioner:

$$\mathcal{M}_S^{-1} := \mathcal{H}_{P,B} \mathcal{S}_P \mathcal{H}_{P,B}^T + \mathcal{H}_{E,B} \mathcal{S}_E \mathcal{H}_{E,B}^T. \quad (3.5)$$

The FETI system (3.4) is considered to be solved using PCG method with left conditioner \mathcal{M}_S (see Algorithm 1). However, since the matrix \mathcal{K}_S is too complicated to be explicitly presented, that is, calculating $\mathcal{K}_S \mathbf{p}_k$ for each k in Algorithm 1 involves solving a Schur complement system with coefficient matrices $\mathcal{S}_{\mathcal{D}}$, which needs implementing PCG method in each PCG step resulting in a multiplicative superposition of PCG iterations.

Algorithm 1 PCG algorithm for solving (3.4)

```

1: Let  $\lambda_h^0 = \mathbf{0}$ 
2: for  $n = 1, 2, \dots, N$  do
3:   Let  $\lambda_h^{(n,0)} := \lambda_h^{n-1}$ ,  $\mathbf{r}_0 := \mathcal{F}_S^n - \mathcal{K}_S \lambda_h^{(n,0)}$ ,  $\mathbf{z}_0 := \mathcal{M}_S^{-1} \mathbf{r}_0$ ,  $\mathbf{p}_0 := \mathbf{z}_0$ 
4:   for  $k = 0, 1, 2, \dots$  until convergence  $\lambda_h^{(n,k)} \rightarrow \lambda_h^n$  do
5:      $\alpha_k = (\mathbf{r}_k, \mathbf{z}_k) / (\mathbf{p}_k, \mathcal{K}_S \mathbf{p}_k)$ 
6:      $\lambda_h^{(n,k+1)} := \lambda_h^{(n,k)} + \alpha_k \mathbf{p}_k$ 
7:      $\mathbf{r}_{k+1} = \mathbf{r}_k - \alpha_k \mathcal{K}_S \mathbf{p}_k$ 
8:      $\mathbf{z}_{k+1} = \mathcal{M}_S^{-1} \mathbf{r}_{k+1}$ 
9:      $\beta_k = (\mathbf{r}_{k+1}, \mathbf{z}_{k+1}) / (\mathbf{r}_k, \mathbf{z}_k)$ 
10:     $\mathbf{p}_{k+1} = \mathbf{z}_{k+1} + \beta_k \mathbf{p}_k$ 
11:   end for
12: end for
Output:  $\lambda_h^n$  ( $n = 1, 2, \dots, N$ )
```

This theoretical fact is far from satisfactory for computation. A generalized implementation proposed in ?? will naturally avoid the multiplicative superposition of PCG iterations, that is, we do not distinguish between interior (including boundary) and interface points, and correspondingly we follow the idea for constructing the FETI Dirichlet preconditioner (3.5) to defined an analogous preconditioner for solving the generalized system.

3.2. A Generalized Implementation. As the last paragraph in ?? describes, to solve (3.4) will unavoidably treat several Schur complement systems, where the PCG algorithm is needed. Here we consider not distinguishing interior and interface points, that is, the following Schur complement system:

$$\mathcal{K}_A \boldsymbol{\lambda}_h^n = \mathcal{F}_A, \quad (3.6)$$

where

$$\begin{aligned} \mathcal{K}_A &= [\mathcal{H}_P^* \quad \mathcal{O}] \begin{bmatrix} \mathcal{A}_P^* & (\mathcal{B}_P^*)^T \\ \mathcal{B}_P^* & -\mathcal{C}_P^* \end{bmatrix}^{-1} \begin{bmatrix} (H_P^*)^T \\ \mathcal{O} \end{bmatrix} + [\mathcal{H}_E \quad \mathcal{O}] \begin{bmatrix} \mathcal{A}_E & \mathcal{B}_E^T \\ \mathcal{B}_E & -\mathcal{C}_E \end{bmatrix}^{-1} \begin{bmatrix} \mathcal{H}_E^T \\ \mathcal{O} \end{bmatrix}, \\ \mathcal{F}_A &= [\mathcal{H}_P \quad \mathcal{O}] \begin{bmatrix} \mathcal{A}_P^* & (\mathcal{B}_P^*)^T \\ \mathcal{B}_P^* & -\mathcal{C}_P^* \end{bmatrix}^{-1} \begin{bmatrix} \mathcal{F}_{P,*}^n \\ \mathcal{Z}^n \end{bmatrix} + [\mathcal{H}_E \quad \mathcal{O}] \begin{bmatrix} \mathcal{A}_E & \mathcal{B}_E^T \\ \mathcal{B}_E & -\mathcal{C}_E \end{bmatrix}^{-1} \begin{bmatrix} \mathcal{F}_E^n \\ \mathcal{O} \end{bmatrix}. \end{aligned}$$

It can be verified by Sylvester's law that \mathcal{K}_A is also symmetric and positive definite. Analogously, we consider the following preconditioner:

$$\mathcal{M}_A^{-1} := [\mathcal{H}_P^* \quad \mathcal{O}] \begin{bmatrix} \mathcal{A}_P^* & (\mathcal{B}_P^*)^T \\ \mathcal{B}_P^* & -\mathcal{C}_P^* \end{bmatrix}^{-1} \begin{bmatrix} (H_P^*)^T \\ \mathcal{O} \end{bmatrix} + [\mathcal{H}_E \quad \mathcal{O}] \begin{bmatrix} \mathcal{A}_E & \mathcal{B}_E^T \\ \mathcal{B}_E & -\mathcal{C}_E \end{bmatrix}^{-1} \begin{bmatrix} \mathcal{H}_E^T \\ \mathcal{O} \end{bmatrix}. \quad (3.7)$$

Analogously, the generalized FETI system (3.6) is considered to be solved using PCG method with left conditioner \mathcal{M}_A (see Algorithm 2). In actuality, \mathcal{M}_A^{-1} can be written in

$$\mathcal{M}_A^{-1} = \mathcal{H}_{P,B} \mathcal{A}_{P,BB} \mathcal{H}_{P,B}^T + \mathcal{H}_{E,B} \mathcal{A}_{E,BB} \mathcal{H}_{E,B}^T.$$

Systems (3.6) has the same solution as (3.2). The difference between \mathcal{M}_A and \mathcal{M}_S is that \mathcal{M}_S has the Schur complement term

$$\mathcal{H}_{P,B} \mathcal{A}_{P,IB} \mathcal{A}_{P,II}^{-1} \mathcal{A}_{P,IB}^T \mathcal{H}_{P,B}^T + \mathcal{H}_{E,B} \mathcal{A}_{E,IB} \mathcal{A}_{E,II}^{-1} \mathcal{A}_{E,IB}^T \mathcal{H}_{E,B}^T,$$

which implies that \mathcal{M}_A has lower cost of computation resource, that is, if we consider solving each subproblem in each subdomain using Schur complement method, it is necessary to adopt PCG algorithm in each iteration. However, the double PCG iterations implies multiplicative maximum number of iterations, which means that the scale of stiffness equations must not be too large in order to reduce the computational costs.

Algorithm 2 PCG algorithm for solving (3.6)

```

1: Let  $\boldsymbol{\lambda}_h^0 = \mathbf{0}$ 
2: for  $n = 1, 2, \dots, N$  do
3:   Let  $\boldsymbol{\lambda}_h^{(n,0)} := \boldsymbol{\lambda}_h^{n-1}$ ,  $\mathbf{r}_0 := \mathcal{F}_A^n - \mathcal{K}_A \boldsymbol{\lambda}_h^{(n,0)}$ ,  $\mathbf{z}_0 := \mathcal{M}_A^{-1} \mathbf{r}_0$ ,  $\mathbf{p}_0 := \mathbf{z}_0$ 
4:   for  $k = 0, 1, 2, \dots$  until convergence  $\boldsymbol{\lambda}_h^{(n,k)} \rightarrow \boldsymbol{\lambda}_h^n$  do
5:      $\alpha_k = (\mathbf{r}_k, \mathbf{z}_k) / (\mathbf{p}_k, \mathcal{K}_A \mathbf{p}_k)$ 
6:      $\boldsymbol{\lambda}_h^{(n,k+1)} := \boldsymbol{\lambda}_h^{(n,k)} + \alpha_k \mathbf{p}_k$ 
7:      $\mathbf{r}_{k+1} = \mathbf{r}_k - \alpha_k \mathcal{K}_A \mathbf{p}_k$ 
8:      $\mathbf{z}_{k+1} = \mathcal{M}_A^{-1} \mathbf{r}_{k+1}$ 
9:      $\beta_k = (\mathbf{r}_{k+1}, \mathbf{z}_{k+1}) / (\mathbf{r}_k, \mathbf{z}_k)$ 
10:     $\mathbf{p}_{k+1} = \mathbf{z}_{k+1} + \beta_k \mathbf{p}_k$ 
11:   end for
12: end for
Output:  $\boldsymbol{\lambda}_h^n$  ( $n = 1, 2, \dots, N$ )
```

4. Numerical Results. In this section, we consider several numerical tests cases for validating the computation efficiency of the above algorithms. First we adopt a model that has exact solutions in the poroelasticity subdomain, and from this the exact solutions in the elasticity domain can be manufactured. In this model we consider the two settings of finite element discretization: the $(\mathbf{P}_2\text{-}\mathbf{P}_1\text{-}\mathbf{P}_1\text{-}\mathbf{P}_1, \mathbf{P}_2\text{-}\mathbf{P}_1)$ finite element space and the lowest-order $(\mathbf{P}_1\text{-}\mathbf{P}_1\text{-}\mathbf{P}_1\text{-}\mathbf{P}_1, \mathbf{P}_1\text{-}\mathbf{P}_1)$ finite element space, where the convergence order and the parametric robustness to the Poisson's ratio. Then the Barry-Mercer's problem is focused as a benchmark test problem.

4.1. Test Case 1: Convergence Order Validation. Consider the unit square domain $\Omega = [0, 1] \times [0, 1]$, where $\Omega^P = [0, 1] \times [0, 1/2]$ and $\Omega^E = [0, 1] \times [1/2, 1]$. Time interval and step are set in $T = 10^{-2}$ and $\tau = 10^{-4}$. We set the exact solution of \mathbf{u}, p in Ω^P in the following:

$$\mathbf{u}_P = \begin{bmatrix} \sin(2\pi x) \sin(2\pi y) \\ \sin(2\pi x) \sin(2\pi y) \end{bmatrix}, \quad p = \sin(\pi x) \sin(\pi y).$$

To guarantee that the transmission condition on Γ holds, we consider the following manufactured solutions:

$$\mathbf{u}_E = \mathbf{u}_P + \begin{bmatrix} 0 \\ -\frac{\alpha p(y-1/2)}{\lambda_P + 2\mu_P} \end{bmatrix}.$$

In this test case we set the $(\mathbf{P}_2\text{-}P_1\text{-}P_1\text{-}P_1, \mathbf{P}_2\text{-}P_1)$ finite element space for the spatial discretization of the model. The parametric settings are listed in Table 4.1, where the Poisson's ratio ν_D are multiply set for validating that the model can overcome the “locking” of both displacement and pressure.

Table 4.1: Parameters in ??

Parameter	Description & Value	
E_D	Young's modulus	$E_P = E_E = 10^4$
ν_D	Poisson's ratio	$\nu_P = \nu_E = 0.2, 0.49, 0.499, 0.4999$
λ_D, μ_D	Lamé constants	$\lambda_D = \frac{E_D \nu_D}{(1+\nu_D)(1-2\nu_D)}, \mu_D = \frac{E_D}{1+\nu_D}$
α	Biot-Willis constant	1
c_0	Fluid specific storage coefficient	0.1
\mathbf{K}	Skeleton permeability tensor	$\mathbf{1I}_2$
μ_f	Fluid viscosity	1

We calculated the model problem in respectively 8×8 , 16×16 , 24×24 and 32×32 uniform triangulation meshes, and $L^\infty(L^2)$ errors and convergence orders are shown in Table 4.2. To present the results, we plot the computational results of the displacement \mathbf{u} and pressure p at $\nu_D = 0.2$, $h = 1/16$ and $t = 0.001$ with heatmaps (see Figure 4.1). The results shows the convergence of the numerical model, and the superconvergence occurs for both displacement \mathbf{u} and pressure p , that is, the higher spatial convergence error order than the interpolation error orders of the corresponding finite element spaces.

The following Figure 4.2 presents the errors of displacement \mathbf{u} and pressure p respectively when adopting different Poisson's ratios ν_D . From this we find that the error of \mathbf{u} increases and the error of p is almost unchanged. However, the error of p when $h = 1/8$ and $\nu_D = 0.4999$ is much larger than other test positions. This exception can be explained by the influence of relatively large error of displacement \mathbf{u} (greater than 10^{-2}). We can from the above observations conclude that the model is robust to Poisson's ratio and can overcome the “locking” of both displacement and pressure.

4.2. Test Case 2: Lowest-order Finite Element Space. In this numerical test we consider adopting the lowest-order finite element space, that is, the $(\mathbf{P}_1\text{-}P_1\text{-}P_1\text{-}P_1, \mathbf{P}_1\text{-}P_1)$ finite element space for spatial discretization, and the domain, exact solutions and parameter settings are all the same as test case 1 (see). We calculated again the model problem in respectively 8×8 , 16×16 , 24×24 and 32×32 uniform triangulation meshes, and $L^\infty(L^2)$ errors and convergence orders are shown in Table 4.3. We can find that the model converges like the above settings of $(\mathbf{P}_2\text{-}P_1\text{-}P_1\text{-}P_1, \mathbf{P}_2\text{-}P_1)$ finite element space, and the superconvergence phenomenon that has shown in test case 1 still exists in this lowest-order finite element case.

The following ?? presents the errors of displacement \mathbf{u} and pressure p respectively when adopting different Poisson's ratios ν_D . We can see that the errors of displacement \mathbf{u} and pressure p have the minimal change when ν_D is gradually close to 0.5. However, the error of \mathbf{u} does not show an increasing phenomenon like test case 1, and the error of p at $\nu_D = 0.2$ is much larger than other settings of ν_D . The results totally shows that the model can overcome the “locking” of both displacement and pressure, and has stronger robustness when adopting the lowest-order finite element discretization than what test case 1 has shown.

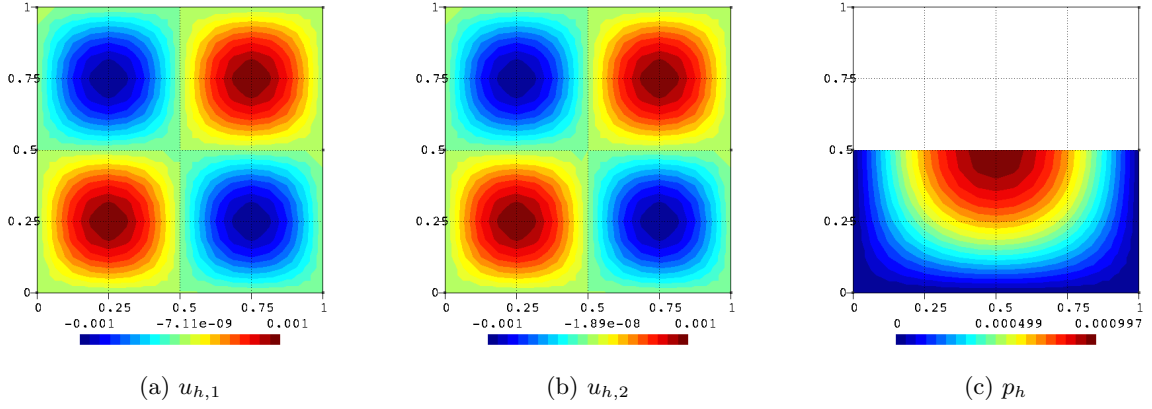
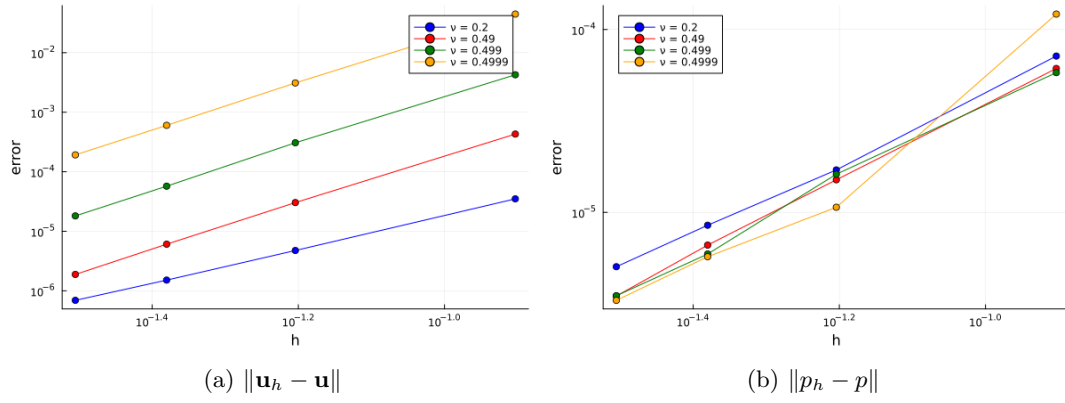
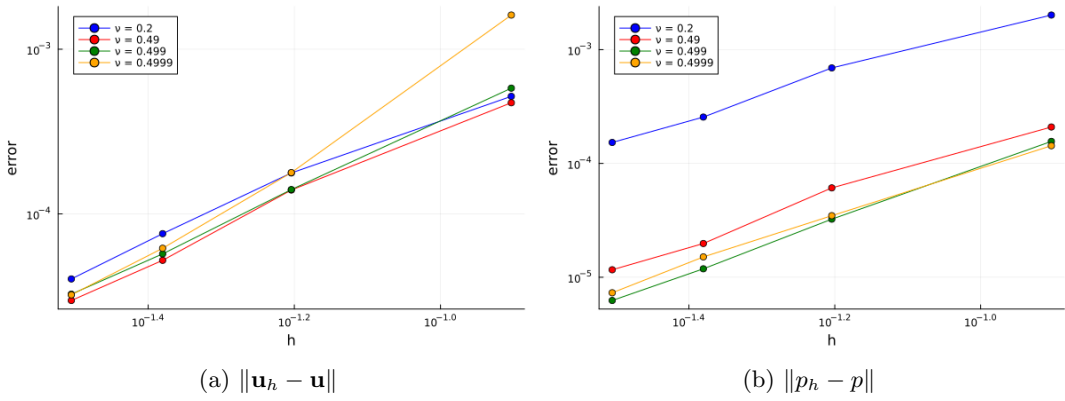
Figure 4.1: Plots of solutions at $\nu = 0.02$, $h = 1/16$ and $t = 0.001$.Figure 4.2: Error plots in $L^\infty(L^2)$ -norm in test case 1Figure 4.3: Error plots in $L^\infty(L^2)$ -norm in test case 2

Table 4.2: Errors in $L^\infty(L^2)$ -norm and convergence order for test case 1

ν	h	$\ \mathbf{u}_h - \mathbf{u}\ $	Order	$\ p_h - p\ $	Order
0.2	1/8	3.4464×10^{-5}	—	8.3059×10^{-5}	—
	1/16	4.9157×10^{-6}	2.8096	1.7016×10^{-5}	2.2872
	1/24	1.5306×10^{-6}	2.8775	7.7335×10^{-6}	1.9322
	1/32	6.8132×10^{-6}	2.8135	4.8641×10^{-6}	1.6297
0.49	1/8	4.4612×10^{-4}	—	5.8174×10^{-5}	—
	1/16	3.0153×10^{-5}	3.8870	1.3567×10^{-5}	2.1003
	1/24	6.0305×10^{-5}	3.9694	6.6025×10^{-6}	1.7762
	1/32	1.9107×10^{-6}	3.9953	3.3601×10^{-6}	2.1071
0.499	1/8	4.8806×10^{-3}	—	5.9630×10^{-5}	—
	1/16	3.1105×10^{-4}	3.9719	1.3508×10^{-5}	2.1422
	1/24	5.9523×10^{-5}	4.0782	6.6926×10^{-6}	1.7693
	1/32	1.8070×10^{-5}	4.1439	3.2951×10^{-6}	2.4106
0.4999	1/8	4.7204×10^{-2}	—	1.1970×10^{-4}	—
	1/16	3.0931×10^{-3}	3.9318	1.4237×10^{-5}	3.0717
	1/24	5.9446×10^{-4}	4.0676	5.8680×10^{-6}	2.1860
	1/32	1.8671×10^{-4}	4.0256	3.9846×10^{-6}	1.3455

Table 4.3: Errors in $L^\infty(L^2)$ -norm and convergence order for test case 2

ν	h	$\ \mathbf{u}_h - \mathbf{u}\ $	Order	$\ p_h - p\ $	Order
0.2	1/8	5.4843×10^{-4}	—	1.9126×10^{-3}	—
	1/16	1.7852×10^{-4}	1.6192	6.4009×10^{-4}	1.5792
	1/24	7.6087×10^{-5}	2.1033	2.9777×10^{-4}	1.8874
	1/32	4.1245×10^{-4}	2.1284	1.4564×10^{-4}	2.4859
0.49	1/8	4.8635×10^{-4}	—	1.9548×10^{-4}	—
	1/16	1.3026×10^{-4}	1.9005	5.5812×10^{-5}	1.8084
	1/24	5.4334×10^{-5}	2.1565	2.0711×10^{-5}	2.4448
	1/32	2.9772×10^{-5}	2.0911	1.1630×10^{-5}	2.0060
0.499	1/8	5.7018×10^{-4}	—	1.5800×10^{-4}	—
	1/16	1.4273×10^{-4}	1.9981	3.1721×10^{-5}	2.3164
	1/24	5.7814×10^{-5}	2.2289	1.2862×10^{-5}	2.2262
	1/32	3.2537×10^{-5}	1.9981	6.2831×10^{-6}	2.4905
0.4999	1/8	1.6353×10^{-3}	—	1.4759×10^{-4}	—
	1/16	1.6725×10^{-4}	3.2894	3.49312×10^{-5}	2.0790
	1/24	6.1010×10^{-5}	2.4872	1.2877×10^{-5}	2.4612
	1/32	3.2578×10^{-5}	2.1808	6.2396×10^{-6}	2.5185

4.3. Test Case 3: Barry–Mercer’s Problem. In this numerical test we consider the Barry–Mercer’s problem as the benchmark test problem. We also consider the unique square domain defined in ?? (see Figure 4.4a), and $T = 1$. Source terms and boundary conditions are set in the following.

$$\begin{aligned}
\mathbf{f} &\equiv \mathbf{0}, \\
z &\equiv 0, \\
p &= 0 && \text{on } \partial\Omega^P \cap (\Gamma_1 \cup \Gamma_3), \\
\mathbf{w}(p) \cdot \mathbf{n}_{P \rightarrow E} &= 0 && \text{on } \Gamma,
\end{aligned}$$

$$\begin{aligned}
p &= p_2 && \text{on } \Gamma_2, \text{ where } p_2 = \begin{cases} \sin t & \text{if } 0.2 \leq x \leq 0.8 \\ 0 & \text{otherwise} \end{cases} \\
u_1 &= 0 && \text{on } \Gamma_1 \cup \Gamma_3, \\
u_2 &= 0 && \text{on } \Gamma_2 \cup \Gamma_4, \\
\tilde{\sigma}_P(\mathbf{u}_P, \xi_P) \cdot \mathbf{n}_P &= (0, \alpha p_2)^T && \text{on } \Gamma_2, \\
\mathbf{u}_0(\mathbf{x}) &= \mathbf{0}, \\
p_0(\mathbf{x}) &= 0,
\end{aligned}$$

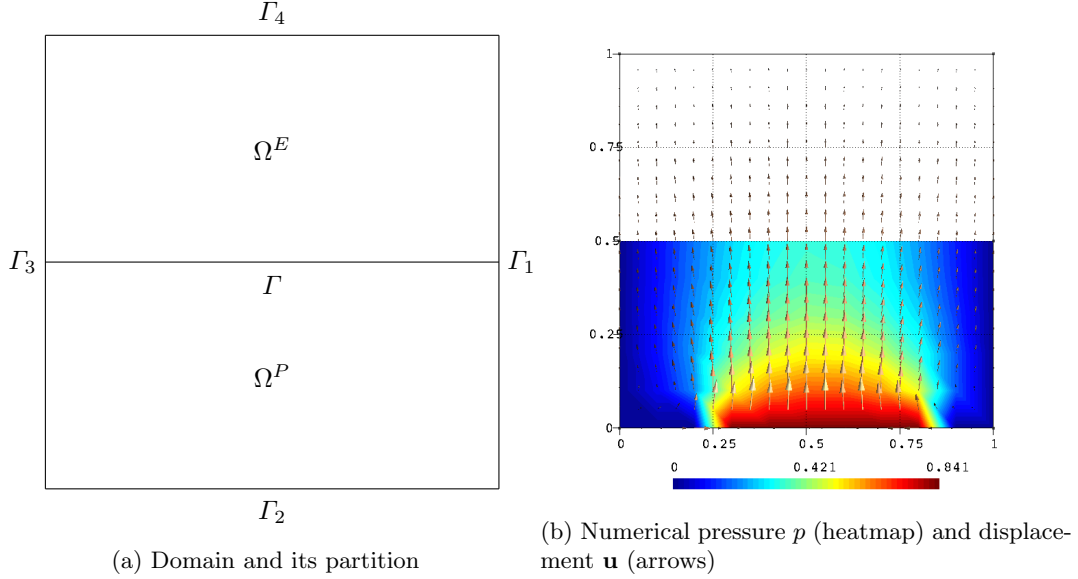


Figure 4.4: Domain and numerical result for Barry-Mercer's problem

Note that Barry–Mercer's problem has a unique solution that is given by a series (see [23]), and the manufactured solutions in the elasticity domain can be found using the similar technique in ?? . The computational result under the above settings is shown in Figure 4.4b, where the computed pressure in $[0, 1] \times [0, 1/2]$ is shown by a heatmap and the computed displacement in $[0, 1] \times [0, 1]$ is displayed by arrows. The results show that algorithm 1 and algorithm 2 performs well in computing the Barry-Mercer's problem and does not produce any oscillation in computed pressure.

5. Conclusion. In this paper, we proposed an time-efficient algorithm for solving a coupled poroelasticity and elasticity model with multiphysics finite element approximation in a Lagrange multiplier framework. The fully-discretized problem was reconstructed into a saddle point form, and then the specifically designed multiphysics FETI method was adopted for iterative solving. Numerical tests showed that the algorithm possess the time efficiency and high accuracy in computational results, and the “locking” phenomenon was overcome according to the results under different Poisson's ratios. And the domain decomposition method revealed the strong potential for parallelization, and strategies and techniques for constructing the algorithm can be applied to the more complicated multiphysics domain decomposition problems.

REFERENCES

- [1] J. ABDI, F. HADAVIMOGHADDAM, M. HADIPOOR, AND A. HEMMATI-SARAPARDEH, *Modeling of CO₂ adsorption capacity by porous metal organic frameworks using advanced decision tree-based models*, Scientific reports, 11 (2021), p. 24468.
- [2] P. F. ANTONIETTI AND B. AYUSO, *Schwarz domain decomposition preconditioners for discontinuous galerkin approximation of elliptic problems: non-overlapping case*, ESAIM: Mathematical Modelling and Numerical Analysis, 41 (2007), pp. 21–54.
- [3] M. A. BIOT, *General theory of three-dimensional consolidation*, Journal of applied physics, 12 (1941), pp. 155–164.
- [4] D. BOFFI, F. BREZZI, M. FORTIN, ET AL., *Mixed finite element methods and applications*, vol. 44, Springer, 2013.
- [5] H. CHEN AND Z. GE, *Physical information neural networks for 2D and 3D nonlinear biot model and simulation on the pressure of brain*, Journal of Computational Physics, 490 (2023), p. 112309.
- [6] H. CHU, L. F. PAVARINO, AND S. ZAMPINI, *Block bddc/feti-dp preconditioners for three-field mixed finite element discretizations of biot's consolidation model*, arXiv preprint arXiv:2504.04859, (2025).
- [7] O. COUSSY, *Poromechanics*, John Wiley & Sons, 2004.
- [8] Z. DAI, H. VISWANATHAN, T. XIAO, R. MIDDLETON, F. PAN, W. AMPOMAH, C. YANG, Y. ZHOU, W. JIA, S.-Y. LEE, ET AL., *CO₂ sequestration and enhanced oil recovery at depleted oil/gas reservoirs*, Energy Procedia, 114 (2017), pp. 6957–6967.
- [9] X. FENG, Z. GE, AND Y. LI, *Analysis of a multiphysics finite element method for a poroelasticity model*, IMA Journal of Numerical Analysis, 38 (2018), pp. 330–359.
- [10] Y. FENG AND A. FIROOZABADI, *Phase-field simulation of hydraulic fracturing by CO₂ and water with consideration of thermo-poroelasticity*, Rock Mechanics and Rock Engineering, 56 (2023), pp. 7333–7355.
- [11] V. GIRAULT, G. PENCHEVA, M. F. WHEELER, AND T. WILDEY, *Domain decomposition for poroelasticity and elasticity with DG jumps and mortars*, Mathematical Models and Methods in Applied Sciences, 21 (2011), pp. 169–213.
- [12] M. HOCHBRUCK AND A. OSTERMANN, *Exponential integrators*, Acta Numerica, 19 (2010), pp. 209–286.
- [13] J. KOKO AND T. SASSI, *An uzawa domain decomposition method for stokes problem*, in Domain Decomposition Methods in Science and Engineering XIX, Springer, 2010, pp. 383–390.
- [14] K. LEE, M. TAK, AND T. PARK, *The analysis of porous media using the mixed finite element method and the feti method*, Civil-Comp Proceedings, 100 (2012), pp. 1–11.
- [15] K.-J. LEE, M.-H. TAK, AND T.-H. PARK, *The mixed finite element analysis for saturated porous media using feti method*, Journal of the Computational Structural Engineering Institute of Korea, 23 (2010), pp. 693–702.
- [16] P. LEE, *Feti-dp algorithms for 2d biot model with discontinuous galerkin discretization*, in International Conference on Domain Decomposition Methods, Springer, 2022, pp. 351–358.
- [17] F. MAGOULES, P. IVÁNYI, AND B. H. TOPPING, *Non-overlapping schwarz methods with optimized transmission conditions for the helmholtz equation*, Computer Methods in Applied Mechanics and Engineering, 193 (2004), pp. 4797–4818.
- [18] F. MAGOULÈS AND R. PUTANOWICZ, *Optimal convergence of non-overlapping schwarz methods for the helmholtz equation*, Journal of Computational Acoustics, 13 (2005), pp. 525–545.
- [19] T. P. MATHEW, *Domain decomposition methods for the numerical solution of partial differential equations*, Springer, 2008.
- [20] P. NING, Z.-Q. FENG, J. A. R. QUINTERO, Y.-J. ZHOU, AND L. PENG, *Uzawa algorithm to solve elastic and elastic-plastic fretting wear problems within the bipotential framework*, Computational Mechanics, 62 (2018), pp. 1327–1341.
- [21] P. J. PHILLIPS AND M. F. WHEELER, *A coupling of mixed and continuous Galerkin finite element methods for poroelasticity I: the continuous in time case*, Computational Geosciences, 11 (2007), pp. 131–144.
- [22] —, *A coupling of mixed and continuous Galerkin finite element methods for poroelasticity II: the discrete-in-time case*, Computational Geosciences, 11 (2007), pp. 145–158.
- [23] —, *Overcoming the problem of locking in linear elasticity and poroelasticity: an heuristic approach*, Computational Geosciences, 13 (2009), pp. 5–12.
- [24] K. TERZAGHI, *Theoretical soil mechanics*, John Wiley & Sons, Inc., 1943.
- [25] G. S. YAN'KOVA, A. A. CHEREVKO, A. K. KHE, O. B. BOGOMYAKOVA, AND A. A. TULUPOV, *Study of hydrocephalus using poroelastic models*, Journal of Applied Mechanics and Technical Physics, 61 (2020), pp. 14–24.